

Finite element modeling of human skin using an isotropic, nonlinear elastic constitutive model

Jeffrey E. Bischoff, Ellen M. Arruda*, Karl Grosh

Department of Mechanical Engineering and Applied Mechanics, University of Michigan, 2350 Hayward, 2250 G.G. Brown, Ann Arbor, MI 48109-2125, USA

Accepted 30 December 1999

Abstract

The collagen network in skin is largely responsible for the nonlinear mechanical stress-strain response of skin. We hypothesize that the force-stretch response of collagen is governed by the entropics of long-chain molecules. We show that a constitutive model derived from the statistical mechanics of long-chain molecules, corresponding to the fibrous collagen network in skin, captures the mechanical response of skin. A connection between the physiologically meaningful parameters of network molecular chain density and free length of collagen fibers and the constitutively significant parameters of initial modulus and limiting stretch is thus established. The relevant constitutive law is shown to have predictive capabilities related to skin histology by replicating *in vivo* and *in vitro* experimental results. From finite element simulations, this modeling approach predicts that the collagen network in hypertrophic scars is more dense and the constituent collagen fibers have shorter free lengths than in healthy skin. Additionally, the model is shown to predict that as rat skin ages, collagen network density increases and fiber free length decreases. The importance of knowledge of the *in situ* stress state for analyzing skin response and validating constitutive laws is also demonstrated. © 2000 Elsevier Science Ltd. All rights reserved.

Keywords: Skin; Constitutive modeling; Finite element analysis; Anisotropy; Extensometer

1. Introduction

Human skin is a heterogeneous material composed of collagen and elastin fibers in a proteoglycan matrix. Acting together, these components are responsible for the mechanical behavior of skin as manifested in stress–strain curves. These curves are characterized by a low-stiffness region at small strains followed by a dramatic increase in stiffness as the strain becomes large (Payne, 1991). It is generally accepted that during the initial, low-stiffness region, the collagen fibers align themselves parallel to the maximum stretch direction while either the elastin (Clark et al., 1996; Sanders et al., 1995; Daly, 1982) and/or the proteoglycan matrix (Pereira et al., 1991) provides resistance to deformation. Once the collagen fibers are sufficiently aligned, further extension of the skin requires extension of the collagen fibers, resulting in a significant increase in skin stiffness.

The most popular instrument for determining the mechanical properties of skin *in vivo* has been the extensometer, characterized by two tabs glued to the skin and driven apart from each other. The extensometer has been used both for studying the directional properties of skin (Ferguson and Barbenel, 1981; Alexander and Cook, 1977; Stark, 1977) as well as for clinical evaluation of healthy and diseased skin (Clark et al., 1996, 1987; Leung et al., 1984; Burlin et al., 1977). Various researchers have used *in vitro* tests to determine properties of healthy (Oxlund et al., 1988; Lanir and Fung, 1974) and burned (Dunn et al., 1985) skin.

Attempts to model the mechanical behavior of skin have focused on specific behavioral aspects of the tissue, such as viscoelasticity (Barbenel and Evans, 1977; Christensen et al., 1977) or nonlinear elasticity (Alexander and Cook, 1977). Quasistatic viscoelastic effects are only appreciable at nonphysiologic stress levels however (Daly, 1982; Wilkes et al., 1973). Alexander and Cook (1977) used a phenomenological nonlinear strain energy function to model skin, but their results did not speak to the histologic basis for the observed behavior. Others have focused on developing microstructurally based

* Corresponding author. Tel.: 001-734-763-5328; fax: 001-734-647-3170.

E-mail address: arruda@engin.umich.edu (E.M. Arruda).

models to explain specific traits of the bulk tissue response directly attributable to one component of the tissue, such as the collagen fibers (Haut and Little, 1972). However, this model is applicable to single collagen fibers, and the constitutive law for individual fibers has not yet been incorporated into a network formulation to model bulk tissue behavior.

We hypothesize that since the mechanical behavior of skin at large stretches is dominated by the macromolecular collagen network, a constitutive model based on the entropy change upon stretching of long-chain molecules using physiologically meaningful parameters to represent the collagen network in skin accurately models the elastic behavior of skin. The recent success of statistical mechanics models to describe stretching of DNA (Marko and Siggia, 1995) motivates this hypothesis. This modeling approach is fully compliant with the rubrics of continuum mechanics and results in a specific form for the strain energy density. Consequently, by incorporating this constitutive law into a finite element simulation, results from various experiments can be compared, and changes in a model parameter associated with a skin property such as collagen density predict a change in skin histology between two samples. Additionally, we hypothesize that anisotropic behavior of skin is modeled using an initially isotropic constitutive law that develops anisotropy in the presence of an anisotropic stress state.

2. Methods

Experiments in the literature were sought to provide data necessary to estimate the material constants inherent to the constitutive law and to provide a basis for comparison with finite element predictions. Details about the modeling techniques and the experimental data that served as the bases for the simulations are as follows.

Finite element simulations were performed using ABAQUS/Standard Version 5.7, a commercially available finite element software package produced by Hibbitt, Karlsson & Sorensen, Inc (Hibbitt, 1997). Three- or four-node linear, plane stress elements (ABAQUS element types CPS3 and CPS4, respectively) were used for all simulations. Quasi-static simulations allowing for nonlinearities arising from both the constitutive law and large geometric deformations were performed. The finite element mesh density was determined through a convergence study on the predicted stress fields, requiring that the stress in the relevant gauge section change by less than 1% upon further mesh refinement.

An initially isotropic rubbery elastic constitutive law developed by Arruda and Boyce (1993) was incorporated into ABAQUS to model skin behavior. This model, referred to as the eight-chain model, was developed to capture the large, three-dimensional stress vs. stretch behavior of

rubbery elastic materials. Here the material parameters of the constitutive law (N , the number of rigid links of length l in the fiber which is thus a measure of the free length $r_0 = \sqrt{N}l$ of the fiber, and $n(1/m^3)$, the network molecular chain density) were recast in terms of appropriate collagen network descriptors (N represents the free length of the collagen fibers, and n represents the collagen fiber density and is directly manifested as the initial skin stiffness) to apply this physically based constitutive model to biological materials. The strain energy density for this model fully adheres to the tenets of continuum mechanics (Malvern, 1969).

The true stress–stretch relation for the eight-chain model is given by

$$\sigma_1 - \sigma_2 = \frac{nk\Theta}{3} \sqrt{N} \mathcal{L}^{-1} \left[\frac{\lambda_c}{\sqrt{N}} \right] \frac{(\lambda_1^2 - \lambda_2^2)}{\lambda_c}, \quad (1)$$

where σ_i is a principal stress component, $k = 1.3807 \times 10^{-23}$ Nm/K is Boltzmann's constant, $\Theta = 298$ K is absolute temperature, \mathcal{L}^{-1} is the inverse Langevin function and λ_c is the chain stretch defined as

$$\lambda_c = \frac{1}{\sqrt{3}} (\lambda_1^2 + \lambda_2^2 + \lambda_3^2)^{1/2}, \quad (2)$$

where the subscripts 1,2,3 represent the three principal stretch directions (Arruda and Boyce, 1993). The Langevin function is defined as $\mathcal{L}(x) \equiv \coth(x) - (1/x)$. As the argument λ_c/\sqrt{N} of the inverse Langevin approaches unity $\mathcal{L}^{-1}[\lambda_c/\sqrt{N}]$ asymptotically increases, resulting in an exponentially increasing stiffness, thereby describing the strain-hardening response of macromolecules. When the chain stretch λ_c reaches \sqrt{N} , this value is called the locking stretch as further increases in strain encounter large increases in stress.

Data were obtained from the literature for two distinct in vitro experiments and one in vivo experiment, as described below. Numerical simulation methods corresponding to each experiment are also discussed.

Dunn et al. (1985) excised normal skin samples and hypertrophic scar (HTS) samples from human cadavers. Uniaxial tensile tests were performed on samples 20 mm long and 10 mm wide. The thickness of each of the specimens was not reported, so a thickness of 1 mm (Payne, 1991) was assumed here. Tests on HTS samples were performed along the long axis of the scars. At each location from which normal skin samples were excised, several specimens at different orientations were tested to account for directional variations in mechanical behavior; only an average response was reported. Data were reported as stress–strain; though not stated in the protocol, it was assumed here that the reported stress was nominal stress, and the strain was converted here to stretch using the logarithmic strain.

Because two planes of symmetry exist in the reported in vitro experimental protocol, appropriate boundary

conditions were applied so that only one quarter of the 20 mm \times 10 mm domain required discretization. Thirty-five equally sized four-node elements (7×5) were used in the model. Though it is not explicitly stated in the experimental protocol, it was assumed that the excised specimens were allowed to completely relax prior to testing, and thus no prestress was applied to the model. Force data were converted to nominal stress by dividing by the initial cross-sectional area used in the simulation (5 mm \times 1 mm).

Belkoff and Haut (1991) excised skin from the backs of rats of various ages. They restored the excised sections to their original dimensions and cut dumbbell-shaped specimens oriented laterally or longitudinally relative to the spine of the rat, with gauge length and gauge width of 22.4 and 4.8 mm, respectively. The samples were allowed to relax and then placed in the grips of a servohydraulic testing machine. The grips were separated until a load of 0.1 N was realized; this grip-to-grip distance was then considered to be the gauge length and was typically 2 mm less than the length of the skin specimen found in situ (Belkoff, 1999). However, exact gauge dimensions were not reported. This highlights the difficulty in correlating constitutive models, which require precise knowledge of strains and the stress levels which give rise to them, with experimental results, where such information is sometimes difficult to obtain. Uniaxial tensile tests were then performed until the specimens failed. The authors recorded load-deformation curves from these tests, performed on specimens taken from rats of ages 1, 1.5, 2, 3, and 4 months. Skin thickness of these specimens varied from 0.8 mm at 1 month to 1.5 mm at 4 months (Belkoff, 1999).

These experiments were simulated using a quarter-plane symmetric model of the dumbbell-shaped specimen given in Belkoff and Haut (1991). Roughly 100 uniform elements were used, including 49 equally sized four-node elements (7×7) in the gauge section. By specifying the longitudinal (σ_{long}) and lateral (σ_{lat}) in vivo principal stresses (prior to excision), the relaxed dimensions of the specimens can be calculated from Eq. (1) by assuming a homogeneous 2D stress state. Estimates of the in vivo stresses are necessary to determine these dimensions, as only the in vivo dimensions are given in the literature. However, the experiment begins from a relaxed state. No information in the literature on the in vivo stresses in rat skin has been found. Thus, it was assumed that rat skin typically functions in the low stretch, linear regime with stretches less than the locking stretch allowing for an elastic response to stress (Wilkes et al., 1973). Accordingly, realistic in vivo preloads on dumbbell-shaped specimens will be seen not to exceed approximately 5 N, which corresponds to roughly 1 MPa using the initial width (4.8 mm) and thickness (varies according to age) of the specimens. A mesh was created using relaxed dimensions and a 0.1 N preload was applied. Subsequent defor-

mations were referenced from the preloaded configuration, which replicated the experimental procedure. It was assumed that the in vivo stress state of rats of the same age were equivalent, and thus the same (anisotropic) prestresses were used whether the applied deformation was in the lateral or longitudinal direction. Anisotropic prestresses resulted in different stress-free dimensions of the dumbbell-shaped lateral- and longitudinal-oriented specimens at a given age, which resulted in an anisotropic constitutive response. These data provide an opportunity to test the predictive ability of this model, in which the values of N , n , σ_{long} , and σ_{lat} were determined for each age from the longitudinal sample and subsequently used to predict the results for the corresponding lateral sample. Note, however, that σ_{lat} has a greater effect on the skin response in the lateral direction compared to the longitudinal direction, and thus, after arriving at values of N , n , and σ_{long} to fit the longitudinal data, σ_{lat} could be varied to improve the fit to the lateral data without significantly compromising the accuracy of the longitudinal fit.

Gunner et al. (1979) applied their version of the extensometer to healthy in vivo skin on the human axilla. The tabs on their instrument were 20 mm long and 10 mm wide, initially spaced 10 mm apart. They presented force-time and extension-time data which were digitized and converted to nominal stress versus stretch by assuming an initial thickness of 1 mm and an initial width equal to the width of the extensometer tabs (10 mm).

A quarter-plane symmetric finite element model was created to simulate this experiment (Fig. 1), a model in which it is assumed that the domain and tabs were aligned with the principal stress axes and therefore no shear boundary forces were present. As skin in vivo is typically under an anisotropic state of stress, uniform but anisotropic initial stresses (σ_{xx} and σ_{yy}) were assigned to each element in the model with concomitant boundary conditions. Daly and Odland (1979) reported that in vivo stress levels in humans usually do not exceed tens of kPa,

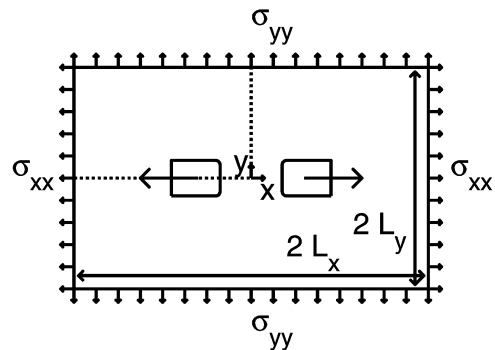


Fig. 1. Geometry used to model in vivo extensometer experiments in which the axes are aligned with the principal stress directions. σ_{xx} and σ_{yy} represent initial stresses used to prestress the model. The dashed lines represent a quarter model used when the model is symmetric in the x - and y - directions (i.e., there are no initial shear stresses).

so σ_{xx} and σ_{yy} were varied in this range. The boundary conditions were applied by transforming the initial stresses (σ_{xx} and σ_{yy}) to forces applied at each boundary node, assuming each node on the boundary to have an area consistent with the boundary nodal distribution. Thus, an equilibrium between boundary nodal loads and initial stresses throughout the domain was achieved. Though the stress field of the in vivo skin samples are unknown, an allowance for this initial stress is physiologically relevant and necessary for successful modeling. Since this test was performed on an in vivo sample, the domain where finite element computations are performed must be truncated in a consistent fashion with appropriate boundary conditions (unlike the in vitro preparations where the computational domain is fixed by the sample size). As such, convergence of the model domain was confirmed by increasing L_x and L_y until a further increase in the domain size did not cause a significant (less than 1%) change in the resulting stress field in the region of interest (the region between the two tabs of the extensometer). According to this protocol, the total mesh size arrived upon was $L_x = 55$ mm by $L_y = 40$ mm. A total of 4290 four-node elements were used (roughly 65×70 , with no elements in the rigid tab region); smaller elements by a factor of 0.95 (relative to their next neighbor) were located closer to the tab edges. Extensometer experiments often give rise to stress concentrations at the trailing edges of the displaced tabs. To minimize numerical errors in simulating these portions of the domain, trailing corners of the tabs were slightly rounded. The tab was then displaced as per extensometer experiments, and stretch predictions were calculated relative to the prestressed model size.

True stress values were extracted from this simulation at a single representative node (located on the centerline midway between the two tabs) for each stretch increment. Nominal stress values were calculated by dividing these true stress values by the stretch parallel to the direction of the applied deformation; the stretch was calculated from the logarithmic strain at that node. These values are referred to as “nodal stress”, and are the stress values that the tissue experiences. In contrast, the “applied stress” values were calculated by dividing the total force on the extensometer tab at each stretch increment by the initial area of the specimen between the tabs (10 mm^2). These estimates from the extensometer do not include the prestress on the tissue and do not account for the nonuniformity of the stress field between the tabs. Initial elastic moduli were calculated from each of these curves to assess the ability of an extensometer to measure an accurate initial elastic modulus. The modulus for either curve was calculated as the slope between the first two data points (superscripts (1) and (2)), $\Delta\sigma/\Delta\varepsilon = (\sigma_{xx}^{(2)} - \sigma_{xx}^{(1)})/(\ln \lambda_x^{(2)} - \ln \lambda_x^{(1)})$.

The parameters (n , N , and lateral and longitudinal prestress when applicable) used in simulations of all three

experiments were determined by trial and error, fitting the predictions to the experimental data according to visual inspection. As n corresponds to an initial modulus and dominates low-stretch behavior, and N represents the square of a locking stretch (limiting extensibility) and dominates large-stretch behavior, simulations are sensitive to these parameters. The use of prestress in the model of the in vivo extensometer experiment reduces the apparent locking stretch and increases the apparent initial modulus, thus affecting the material response at all stretches. Hence, a fit requires the variation of the prestresses in tandem with the material parameters.

3. Results

The simulation of the experiments described in Dunn et al. (1985) closely match their data at low strain (Fig. 2). The simulation parameters are $N = 1.10$ and $n = 5 \times 10^{22}/\text{m}^3$ for normal skin, and $N = 1.05$ and $n = 5 \times 10^{23}/\text{m}^3$ for HTS. The simulation captures the HTS response throughout the domain, whereas the healthy skin data are not well represented at high strains. Because the experimental results for the healthy skin exhibit an asymptotic strain hardening which is less than the hardening characteristic of biological materials, it is possible that an inelastic mechanism such as tearing may have occurred. This nontraditional hardening behavior could also be an artifact of the averaging of data from tests in different directions.

The digitized experimental anisotropic data from Belkoff and Haut (1991) closely match the corresponding finite element simulations (Fig. 3). Each curve in Fig. 3a has a corresponding curve in Fig. 3b produced without changing the material parameters (given in Table 1), the

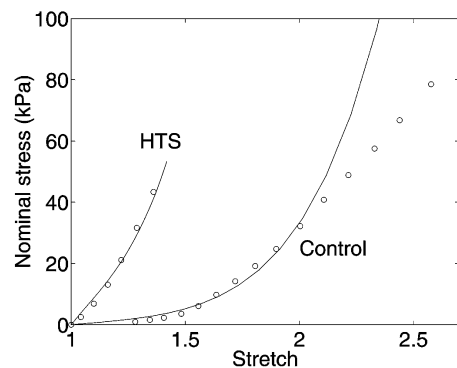


Fig. 2. In vitro, uniaxial test data (indicated by open circles) from human skin under control and hypertrophic scar (HTS) conditions, adapted from Dunn et al. (1985). The corresponding best-fit curves (indicated by solid lines) from finite element simulations use parameters $N = 1.10$ and $n = 5 \times 10^{22}/\text{m}^3$ for control data and $N = 1.05$ and $n = 5 \times 10^{23}/\text{m}^3$ for HTS data. These results indicate that HTS has a higher collagen network density containing fibers of shorter free lengths than in healthy skin.

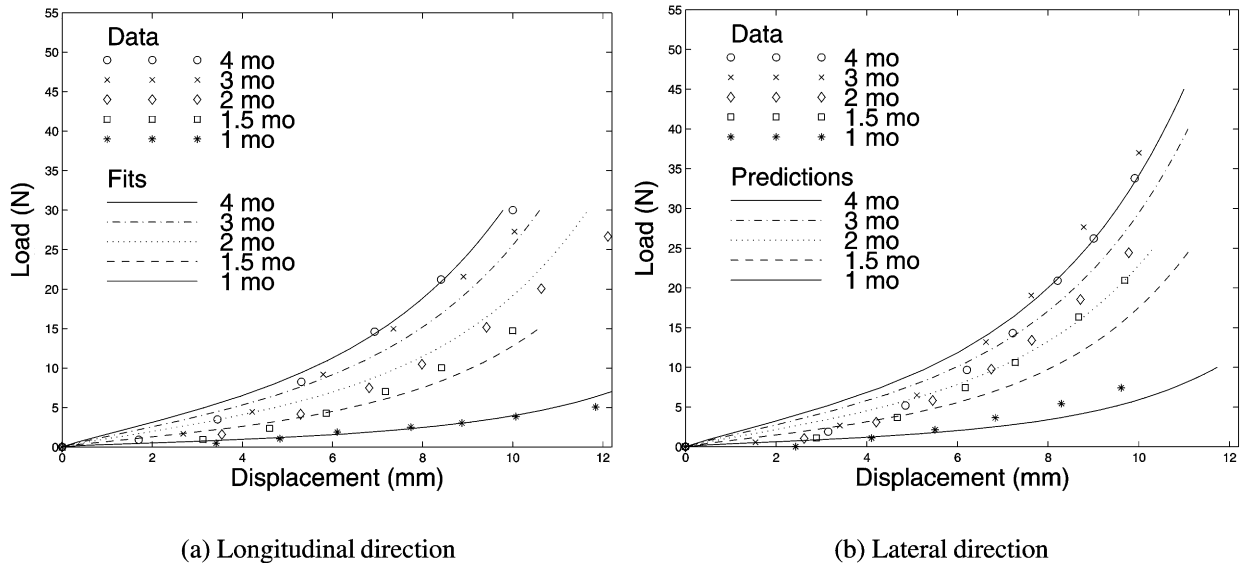


Fig. 3. In vitro, uniaxial test data from rat skin, adapted from Belkoff and Haut (1991), and best-fit curves from finite element simulations, demonstrating good fit to the anisotropic data. Parameters for the fitted curves are given in Table 1. Orientations are with respect to the length of the rat. In both figures, symbols denote data and lines denote fits obtained from simulations. Longitudinal data were used to acquire material constants and the initial stress field from simulations; these values were then used to predict the corresponding responses in the lateral direction.

Table 1
Parameters found from fitting longitudinal data from experiments by Belkoff and Haut (1991) and used to predict their laterally oriented experiments. Curves are shown in Fig. 3

Age (months)	Thickness (mm)	$n(1/m^3)$	N	σ_{lat} (MPa)	σ_{long} (MPa)
1	0.8	0.7×10^{26}	1.40	0.89	0.61
1.5	0.95	0.9×10^{26}	1.23	1.08	0.75
2	1.1	1.2×10^{26}	1.23	0.70	0.49
3	1.3	1.2×10^{26}	1.21	0.67	0.50
4	1.5	1.2×10^{26}	1.20	0.53	0.44

only difference is the orientation of the specimen. As the age of the rat from which the sample is excised increases, the model parameters generally change in a consistent manner (Table 1); the collagen density n increases, whereas the free length of the collagen fibers N decreases. Additionally, the prestresses σ_{lat} and σ_{long} are generally lower at older ages than younger ages, and remain in the small stretch, linear range at each age.

The constitutive response extracted from a simulation of the experiment from Gunner et al. (1979) closely matches the experimental data (Fig. 4). The parameters used in the simulation are $N = 1.2$ and $n = 9.6 \times 10^{23}/m^3$, with a prestress of 51 and 0.5 kPa parallel to and orthogonal to the deformation, respectively. The simulation of this experiment by finite elements, where knowledge of stress and strain is available, demonstrates the inaccuracy of the often-used in vivo extensometer technique to measure true skin response

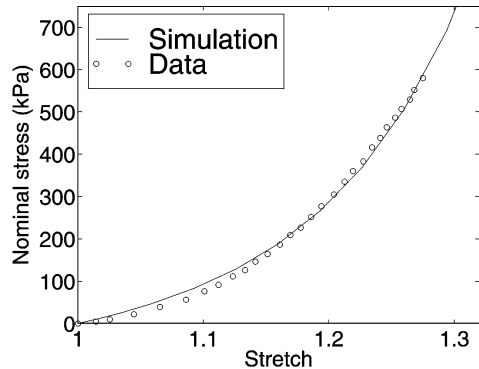


Fig. 4. In vivo extensometer test data from Gunner et al. (1979). Simulation uses parameters $N = 1.2$, $n = 9.6 \times 10^{23}/m^3$, a prestress of 51 kPa in the direction of deformation, and a prestress of 0.5 kPa in the direction orthogonal to deformation.

(Figs. 5 and 6). The deformation from the simulated extensometer test is distinctly not uniaxial, as the normal stress in the direction of the applied deformation is not homogeneous especially near the corner of the extensometer tab (Fig. 5). Hence, measurements based on an assumption of a uniform stress field would be in error. The variation of the applied stress response as measured via the extensometer from that of the actual nodal stress (Fig. 6) highlights the inaccurate initial modulus estimate from the extensometer (697 kPa), an estimate which does not account for the in vivo stress state. The actual initial modulus calculated from the nodal stress response at zero prestress is 102 kPa.

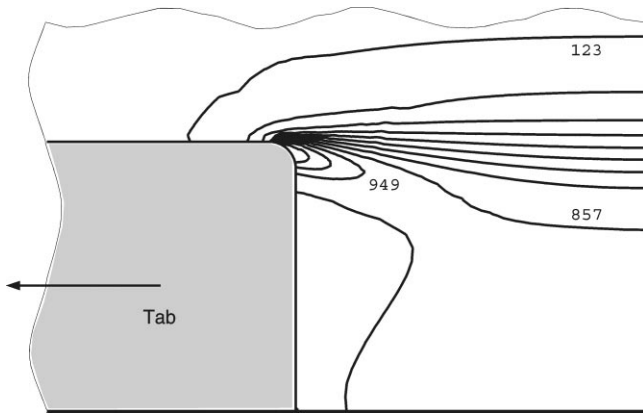


Fig. 5. Contour plot of normal stress in horizontal direction from simulation of in vivo extensometer test data from Gunner et al. (1979), exhibiting extensive stress concentration at the tab corner resulting in a response stiffer than uniaxial tension. Contour values are in kPa. This figure is focused on the region bounded by the tab (shaded portion of the figure) and the axes of symmetry (solid lines on right and bottom of figure).

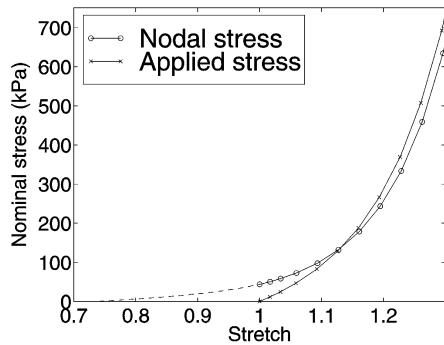


Fig. 6. Nominal stress–stretch data from simulations of in vivo extensometer test data from Gunner et al. (1979). One curve is calculated from the true stress values at a single representative node in the region between the tabs (“Nodal stress”), and the other curve is calculated from the force data from the tabs (“Applied stress”). The dashed line indicates that portion of the stress–stretch curve which is realized during pre-stressing. Failure to account for the prestress in skin will therefore yield incorrect estimates of elastic moduli.

4. Discussion

Previous attempts to model the elastic constitutive response of skin have been successful insofar as data obtained from experiments have been fit using phenomenological strain energy functions (Alexander and Cook, 1977). However, these models have not been applied to data from skin of different histologies to elucidate biological differences between samples. Comparisons between biologically different samples have generally been strictly qualitative (Ferguson and Barbenel, 1981; Stark, 1977) or based on an approximate calculation of the elastic modulus (Clark et al., 1996, 1987; Leung et al., 1984) that are not easily transferable to different experimental con-

figurations. Accordingly, we hypothesized that experimental data from the literature could be modeled using a statistical mechanics-based constitutive model adapted for biological materials by incorporating physiologically meaningful parameters. Additionally, we hypothesized that anisotropic behavior could be modeled using an isotropic constitutive law in an anisotropic stress state. As such, data from various experiments could be contrasted, and the histological bases for differences in their constitutive responses could be explored.

A prestretched, initially isotropic constitutive law incorporated within a finite element model can successfully simulate the anisotropic response of skin obtained from in vivo and in vitro tests (Figs. 2–4). The stress–stretch curves extracted from the simulations closely match those obtained from uniaxial test data on in vitro skin samples averaged over multiple directions (Fig. 2) and from uniaxial test data taken in mutually orthogonal directions (Fig. 3), as well as from an in vivo extensometer test (Fig. 4). The strength of the modeling approach is clear in the simulations for which an anisotropic response is captured in two orthogonal directions without changing material constants (Fig. 3), indicating that skin is either isotropic, or has nearly orthogonal anisotropy. Fig. 3b represents predictions of material responses using material constants estimated from the independent results in Fig. 3a. In fitting the lateral data in Fig. 3b, however, there was some latitude in choosing the prestress in the lateral direction, as this parameter has a greater impact on the material response in the lateral direction as compared to the longitudinal direction.

The use of an anisotropic prestress state allows the initially isotropic constitutive law to model phenomena which otherwise would be beyond the scope of the model in two important ways. First, data obtained from in vivo tests sometimes reach the strain hardening region at lower measured stretches (Fig. 4) than in in vitro tests (Lanir and Fung, 1974), but a prestress in the simulation can account for this. Also, an isotropic model can predict an anisotropic response provided an anisotropic stress state is used (Fig. 3). However, in vitro data with no prestress (Lanir and Fung, 1974) that nevertheless demonstrate anisotropy cannot be simulated by this current model.

The constitutive parameters in the model used here, N (fiber-free length) and n (network collagen chain density), possess physiological meaning. The model parameters for the data from Dunn et al. (1985) imply that the collagen fibers in HTS tissue have shorter free lengths and the collagen network is more dense than in normal tissue, conclusions supported by histological examination and comparison of scar and normal tissue (Dunn et al., 1985). The fitted parameters for data obtained from Belkoff and Haut (1991), given in Table 1, indicate that as the age of the skin increases the collagen fibers are slightly less extensible, the collagen density is higher, and the

resting stress level decreases. The loss in extensibility may arise from additional crosslinking during aging or from increased collagen alignment during growth. Higher network fiber density is consistent with either the production of collagen (in accordance with the histological evidence of Flandin et al., 1981) or increased crosslinking. These observations make intuitive sense when applied to data obtained from an immature animal, in which the morphology of skin is constantly changing as the animal grows to better accommodate and reduce *in vivo* stresses. From simulations of human skin (Figs. 2 and 4), the relatively low values of the fiber-free length ($N = 1.05\text{--}1.2$) indicate that the collagen fibers are aligned, supported by histological observations of skin (Wilkes et al., 1973). Results also indicate that the fiber-free lengths (N) of collagen in rat skin and human skin are comparable ($N = 1.05\text{--}1.4$), but the network density (n) in rat skin is several orders of magnitude greater than in human skin. Additionally, the *in vivo* stresses in rat skin are larger than those in human skin. No histologic data to support or refute these observations have been found in the literature.

Modeling data from extensometer tests using the finite element method is necessary because such experiments do not create a uniform stress field (Fig. 5) from which simple metrics such as an initial modulus of elasticity can be extracted. Neglecting the pre-existing stress field is shown to skew calculations of an initial elastic modulus (Fig. 6). At low stretch (< 1.13), the applied stress inferred from extensometer measurements is lower than the nodal stress in simulations. At larger stretches (> 1.13), the stresses inferred from the extensometer measurements exceed the true nodal stresses. Before any deformation is applied by an extensometer, the skin is in a state of stress. However, it is not possible for the extensometer to capture this information unless special techniques are performed beforehand to estimate the underlying stress field.

The success of the constitutive model used in this analysis to simulate the mechanical behavior of skin is largely due to the significant effect that the collagen network has on the large deformation response of skin. As the model is based on the statistical mechanics of long-chain molecules, any effects of the proteoglycan ground substance on the mechanical response cannot be modeled using the current constitutive law. Additionally, this law is strictly elastic; there is no time-dependent behavior. As such, viscoelastic properties of skin cannot be modeled. However, the effects of proteoglycans (and elastin) on the mechanical response of skin are significant only in the small strain response (Pereira et al., 1991), and viscoelastic effects are only appreciable at stress levels generally not seen *in vivo* (Daly, 1982) and do not affect the tensile stiffness of collagen-based tissues (Schmidt et al., 1990). As such, neglecting these effects in order to model the static response of skin to large deformations

does not seem to negatively impact the success of the model. The presence of material anisotropy in the collagen network, however, can contribute to anisotropic mechanical behavior (Lanir and Fung, 1974), and material anisotropy needs to be incorporated to develop a more robust model.

In summary, we have shown that a constitutive law based on the statistical mechanics of long-chain molecules accurately captures the mechanical behavior of skin in a variety of modes of deformation. By formulating the constitutive law in terms of physiologically meaningful parameters, changes in the histology of skin (such as collagen density and fiber length) are reflected in the parameters of the model. Additionally, finite element simulations have shown that an understanding of the stress state of a nonlinear material such as skin is critical to accurate modeling, and that care must be taken in interpreting results from extensometer experiments. Since some anisotropy (permanent collagen fiber alignment) appears to be present when skin is unloaded, an anisotropic, nonlinear elastic–plastic constitutive model is needed for greater modeling success. Efforts are underway to expand the modeling approach used here to describe the evolution of material anisotropy, as well as stress-assisted skin growth. To further develop such a constitutive model for use in skin mechanics research, and to test the physiologic meaning of the constitutive model parameters, it is necessary to apply techniques that allow for the accurate assessment of the *in vivo* stress–strain field, as well as for measurements of the fiber density and orientation, within *in vivo* skin.

Acknowledgements

Support for this work was provided by a Graduate Research Fellowship to J.E.B. by the National Science Foundation, and is gratefully acknowledged.

References

- Alexander, H., Cook, T.H., 1977. Accounting for natural tension in the mechanical testing of human skin. *Journal of Investigative Dermatology* 69, 310–314.
- Arruda, E.M., Boyce, M.C., 1993. A three-dimensional constitutive model for the large stretch behavior of rubber elastic materials. *Journal of the Mechanics and Physics of Solids* 41 (2), 389–412.
- Barbenel, J.C., Evans, J.H., 1977. The time-dependent mechanical properties of skin. *Journal of Investigative Dermatology* 69, 318–320.
- Belkoff, S.M., 1999. Personal communication.
- Belkoff, S.M., Haut, R.C., 1991. A structural model used to evaluate the changing microstructure of maturing rat skin. *Journal of Biomechanics* 24 (8), 711–720.
- Burlin, T.E., Hutton, W.C., Ranu, H.S., 1977. A method of *in vivo* measurement of the elastic properties of skin in radiotherapy patients. *Journal of Investigative Dermatology* 69, 321–323.

- Christensen, M.S., Hargens III, C.W., Nacht, S., Gans, E.H., 1977. Viscoelastic properties of intact human skin: instrumentation, hydration effects, and the contribution of the stratum corneum. *Journal of Investigative Dermatology* 69, 282–286.
- Clark, J.A., Cheng, J.C.Y., Leung, K.S., 1996. Mechanical properties of normal skin and hypertrophic scars. *Burns* 22 (6), 443–446.
- Clark, J.A., Cheng, J.C.Y., Leung, K.S., Leung, P.C., 1987. Mechanical characterization of human postburn hypertrophic skin during pressure therapy. *Journal of Biomechanics* 20 (4), 397–406.
- Daly, C.H., 1982. Biomechanical properties of dermis. *Journal of Investigative Dermatology* 79, 17s–20s.
- Daly, C.H., Odland, G.F., 1979. Age-related changes in the mechanical properties of human skin. *Journal of Investigative Dermatology* 73, 84–87.
- Dunn, M.G., Silver, F.H., Swann, D.A., 1985. Mechanical analysis of hypertrophic scar tissue: Structural basis for apparent increased rigidity. *Journal of Investigative Dermatology* 84, 9–13.
- Ferguson, J., Barbenel, J.C., 1981. Skin surface patterns and the directional mechanical properties of the dermis. In: Payne, P.A., Marks, R. (Eds.), *Bioengineering and the Skin*. MTP Press, pp. 83–92 (Chapter 10).
- Flandin, F., Herbage, D., Buffevant, C., Bazin, S., 1981. Evolution of structural and biochemical properties of rat skin collagen during maturation. *Cell Mol Biol* 27 (6), 677–685.
- Gunner, C.W., Hutton, W.C., Burlin, T.E., 1979. The mechanical properties of skin in vivo — a portable hand-held extensometer. *British Journal of Dermatology* 100, 161–163.
- Haut, R.C., Little, R.W., 1972. A constitutive equation for collagen fibers. *Journal of Biomechanics* 5, 423–430.
- Hibbitt, (Ed.), 1997. *ABAQUS/Standard Users's Manual*, Version 5.7. Hibbitt, Karlsson Sorensen, Inc.
- Lanir, Y., Fung, Y.C., 1974. Two-dimensional mechanical properties of rabbit skin — II. Experimental results. *Journal of Biomechanics* 7, 171–182.
- Leung, K.S., Cheng, J.C.Y., Leung, Y.K., Clark, J.A., Ma, G.F.Y., Leung, P.C., 1984. In vivo study of the mechanical property of postburn hypertrophic scar tissues. *Journal of Burn Care & Rehabilitation* 5 (6), 458–462.
- Malvern, L.E., 1969. *Introduction to the Mechanics of a Continuous Medium*. Prentice-Hall, Inc., Englewood Cliffs, NJ.
- Marko, J.F., Siggia, E.D., 1995. Stretching DNA. *Macromolecules* 28, 8759–8770.
- Oxlund, H., Manschot, J., Viidik, A., 1988. The role of elastin in the mechanical properties of skin. *Journal of Biomechanics* 21 (3), 213–218.
- Payne, P.A., 1991. Measurement of properties and function of skin. *Clinical Physics and Physiological Measurement* 12 (2), 105–129.
- Pereira, J.M., Mansour, J.M., Davis, B.R., 1991. Dynamic measurement of the viscoelastic properties of skin. *Journal of Biomechanics* 24 (2), 157–162.
- Sanders, J.E., Goldstein, B.S., Leotta, D.F., 1995. Skin response to mechanical stress: adaptation rather than breakdown—a review of the literature. *Journal of Rehabilitation Research and Development* 32 (3), 214–226.
- Schmidt, M.B., Mow, V.C., Chun, L.E., Eyre, D.R., 1990. Effects of proteoglycan extraction on the tensile behavior of articular cartilage. *Journal of Orthopaedic Research* 8, 353–363.
- Stark, H.L., 1977. Directional variations in the extensibility of human skin. *British Journal of Plastic Surgery* 30, 105–114.
- Wilkes, G.L., Brown, I.A., Wildnauer, R.H., 1973. The biomechanical properties of skin. *CRC Critical Reviews in Bioengineering*, pp. 453–495.